Synergistic Bimetallic Ru–Pt Catalysts for the Low-Temperature Aqueous Phase Reforming of Ethanol

Zheng Zhao, Lu Zhang and Qiaohua Tan
School of Chemical, Biological, and Materials Engineering, University of Oklahoma, Norman, OK, 73019

Feifei Yang
Collaborative Innovation Center of Chemical Science and Engineering, School of Chemical Engineering and Technology, Tianjin University, Tianjin, 300072, China

Jimmy Faria
Abengoa Research, C/Energía Solar no. 1, Palmas Altas, Seville, 41014, Spain

Daniel Resasco*
School of Chemical, Biological, and Materials Engineering, University of Oklahoma, Norman, OK, 73019

DOI 10.1002/aic.16430
Published online in Wiley Online Library (wileyonlinelibrary.com)

Aqueous phase reforming (APR) of ethanol has been studied over a series of Ru and Pt catalysts supported on carbon and titania, with different metal loadings and particle sizes. This study proposed that, on both metals, ethanol is first dehydrogenated to acetaldehyde, which subsequently undergoes C—C cleavage followed by different paths, depending on the catalyst used. For instance, although monometallic Pt has high selectivity toward H_2 via dehydrogenation, it has a low efficiency for C—C cleavage, lowering the overall H_2 yield. Large Ru particles produce CH_4 through methanation, which is undesirable because it consumes H_2. Small Ru particles have lower activity but higher selectivity toward H_2 rather than CH_4. On these small particles, CO blocks low-coordination sites, inhibiting methanation. The combination of the two metals in bimetallic Ru–Pt catalysts results in improved performance, benefiting from the desirable properties of each Ru and Pt, without the negative effects of either. *AIChE J*, 00: 000–000, 2018
Keywords: aqueous phase reforming, ethanol, particle size effect, C-C cleavage

Introduction

Hydrogen-based technologies play a key role in the development of sustainable, cleaner, more efficient, and lower CO_2 footprint energy systems.[1] Aqueous phase reforming (APR) of biomass-derived oxygenates provides high-yield H_2 production in a single-step catalytic processes at moderate temperatures.[2,3] Bio-ethanol, produced from renewable biomass, is an attractive feedstock for H_2 production, which has been widely used for high-temperature steam reforming over different metal catalysts.[4-7]

In low-temperature ethanol reforming, the primary reaction mechanism involves dehydrogenation upon adsorption, followed by cleavage of the C—C bond to form surface CO, which further reacts via water gas shift (WGS) reaction[7,8] and CH_x species, which can be hydrogenated to produce CH_4. If the surface CO undergoes methanation instead of WGS, the production of hydrogen is greatly inhibited because it not only prevents formation of H_2 but also consumes H_2 to make CH_4. Among the various metals investigated during the last few decades, Pt exhibits one of the highest selectivity toward H_2 and has been often considered as a promising catalyst for APR of oxygenates.[3] However, the low reaction activity of Pt results in insufficient C—C cleavage. By contrast, although Ru has shown lower selectivity toward H_2 production and high yield toward alkanes (especially CH_4) formation via methanation reaction and Fischer–Tropsch synthesis (FTS),[3,9] it also reveals high activity toward C—C bond breaking, which is a desirable reaction to maximize yield. Therefore, designing optimal catalysts for APR of ethanol requires maximizing the efficiency of C—C cleavage, inhibiting the methanation reaction, and facilitating WGS activity.

In this work, we have explored mono- and bimetallic Pt and Ru catalysts supported on carbon and TiO_2. First, particle size effects were investigated over monometallic Ru and Pt catalysts. It was found that small Ru particles exhibit higher selectivity toward H_2 production and lower CH_4 formation than larger Ru particles. To explore the effect of particle size on surface CO dissociation after the C—C cleavage of ethanol, the rate of FTS was compared over the different Ru catalysts. On Pt, selectivity toward CH_4 and C1-oxygenated is higher for smaller particle sizes, but in general, Pt is less active than Ru for C—C cleavage. The comparison of the performance of

Current address: Jimmy Faria, Catalytic Processes and Materials, MESA+ Institute for Nanotechnology, University of Twente, Enschede 7500 AE, The Netherlands

Correspondence concerning this article should be addressed to D. Resasco at resasco@ou.edu

both monometallic metals leads to the investigation of bimetallic Ru–Pt catalysts, which shows synergistic performance, with increased reaction rate for H_2 production and lower rate for CH_4.

Experimental

Catalyst preparation

Supported Ru and Pt catalysts were synthesized by conventional incipient wetness impregnation, followed by high temperature thermal decomposition of the metal precursors. This decomposition was conducted in flowing hydrogen for the carbon-supported catalysts or in flowing air for the TiO_2-supported ones. A series of monometallic Ru catalysts with different metal loadings and supports were prepared by impregnating ruthenium(III) nitrosyl nitrate solution (Sigma-Aldrich, MO, USA, 1.5 wt % Ru) over activated carbon (Sigma-Aldrich) or titanium(IV) oxide (Sigma-Aldrich, ≥99.5%, P25), respectively. The 5% Ru/C (Type 619) was purchased from Alfa Aesar, MA, USA. The monometallic Pt catalysts were prepared by impregnating an aqueous solution of chloroplatinic acid hydrate (H_2PtCl_6, Sigma-Aldrich, ≥99.9%) over the same two supports as above and subsequently dried at 343.15 K, overnight. The thermal decomposition was achieved by heating (in H_2 or air) at 673.15 K for 4 h for $Ru(NO)(NO_3)_3$[10] and at 773.15 K for 3 h for H_2PtCl_6.[11] Bimetallic Ru–Pt catalysts supported on TiO_2 were prepared by sequential impregnation or co-impregnation. The sequential impregnation was carried out by impregnation and decomposition of the first metal precursor followed by loading the second metal precursor. The calcination conditions used were the same as those for the preparation of monometallic catalysts. In the co-impregnation method, the impregnating aqueous solutions were mixtures of ruthenium(III) chloride hydrate (Sigma-Aldrich, 99.98%) and chloroplatinic acid hexahydrate at the desired ratios. The impregnated sample was then dried at 343.15 K overnight followed by calcination in air at 773.15 K for 4 h.[12] Based on the preparation method used, $Ru/Pt/TiO_2$ indicates that Pt was sequentially impregnated over a previously calcined Ru/TiO_2. Likewise, $Pt/Ru/TiO_2$ indicates that Pt was impregnated first and then Ru. By contrast, the co-impregnated bimetallic catalyst is represented as $Ru–Pt/TiO_2$.

Catalyst characterization

N_2 physisorption was performed on supported monometallic Ru and Ru–Pt bimetallic catalysts on a Micromeritics ASAP 2010 unit. Before analysis, the samples were degassed *in situ* at 503.15 K for 24 h. The micropore volume was derived from the *t*-plot method (relative pressure range: 0.2–0.6), and the total pore volume was determined at $p/p_0 = 0.99$.

The transmission electron microscopy (TEM) images were obtained using a JEOL JEM-2100 (JEOL Ltd., MA) transmission electron microscope, operating with an accelerating voltage of 200 kV and equipped with LaB_6 gun. Catalyst samples were prereduced under H_2 flow at 523.15 K for 3 h before depositing them on carbon-coated copper TEM grids. From the TEM images, metal particle size distributions were obtained by analysis with ImageJ software.[13]

X-ray powder diffraction (XRD) patterns for monometallic Pt, Ru, and bimetallic Pt–Ru catalysts were collected on a D8 Series II X-ray Diffractometer (Bruker AXS, WI, USA), using K radiation generated at 40 kV and 35 mA. Prior to the measurements, the samples were reduced *ex situ* under pure H_2 at 523.15 K for 3 h. The scans covered the 2θ range from 20 to 80°.

Reaction procedure

The APR of ethanol was conducted in the liquid phase, in a 160 mL high-pressure Parr reactor (Model 4564), operated at high temperature 523.15 K in batch mode. In each run, 80 mL of deionized water and 100–200 mg of catalysts were placed in the vessel to perform the catalyst reduction under 1.38 MPa of H_2 at 523.15 K,[12,14] for 2 h. Subsequently, the reactor was cooled down to room temperature and purged with Ar. At this point, 20-mL solution consisted of 15 mL ethanol (Sigma-Aldrich, ≥99.5%), and 5-mL water were injected into the aqueous solution. The overall volume of reactants is 100 mL, corresponding to an ethanol concentration of 15 vol %, which was the same for all reaction runs. By injecting Ar, the system was pressurized to 1.38 MPa, which served as an internal standard for gas composition analysis. Mechanical stirring was started at 600 rpm, and the temperature was raised to the desired value of 523.15 K. After holding the temperature at 523.15 K for a period of time, known as the reaction period, the stirring was stopped and the reactor was quenched to room temperature. The gas phase products were collected in a single-ended miniature sample cylinder and quantitatively analyzed using a Carle Series 400 AGC (Chandler Engineering, OK) equipped with TCD. Liquid products were qualitatively identified using a Shimadzu GCMS-QP2010S, (Shimadzu Corp., MD) equipped with a Zebron ZB-1701 (Phenomenex Inc., CA) column and quantified using an Agilent 7890B GC-FID, (Agilent, CA) equipped with a Zebron ZB-WAXplus (Phenomenex Inc., CA) column.

The aqueous phase FTS was carried out as an additional probe reaction. For this, 100 mg of 5% Ru/C or 150 mg of 0.5% Ru/C were reduced in 100 mL of water under 1.38 MPa of H_2 and 523.15 K for 2 h. Then, the system was cooled down and purged with N_2 before introduction of the reactant gas mixture, which contained a H_2 and CO at a molar ratio of 5 and 1.38 MPa. The FTS was conducted at 523.15 K for 17 h. The gas phase products were analyzed using Carle Series 400 AGC, equipped with a TCD and on an Agilent GC-MS, (Agilent, CA) equipped with a J&W HP-PLOT Q (Agilent, CA) column; the liquid phase products were identified using Shimadzu GCMS-QP2010S, equipped with a Zebron ZB-1701 column.

Ethanol conversion and H_2 production rate for each catalyst are defined as follows:

$$\text{Conversion}\,(\%) = \frac{(\text{mole of reactant reacted})}{(\text{mole of reactant fed})} \times 100\% \quad (1)$$

$$\text{Rate of hydrogen production} = \frac{(\text{mole of } H_2 \text{ produced})}{(\text{mass of catalyst}) \times \text{time}} \quad (2)$$

Results and Discussion

Catalysts characterization

The surface area, pore volume, and average particle size of the various catalysts investigated are presented in Table 1. The surface areas for the C-supported catalyst series are greater than 500 m^2/g, whereas those of the TiO_2-supported series are less than 50 m^2/g. The TiO_2 utilized in the catalyst synthesis is P25, which is a mixture of anatase and rutile phases. Because the anatase phase is less stable than the rutile phase upon heating, the higher calcination temperature (500°C) used

Table 1. Characterization of Ru Series Catalysts

Sample	Surface area (m^2/g)	Pore volume (cm^3/g)	Particle size (nm)
5% Ru/C	585	0.42	3.3
0.5% Ru/C	867	0.68	1.4
2.6% Ru/TiO_2	51	0.25	3.9
0.5% Ru/TiO_2	52	0.20	1.7
1% Ru–2% Pt/TiO_2	33	0.10	2.3

for the bimetallic catalyst may have led to partial collapse of the pore structure and loss of overall surface area,[12,15] as observed in Table 1.

The TEM images and particle size distributions are shown in Figure 1. It can be seen that varying metal loading on the different supports resulted in significant differences in particle size. For instance, the samples with higher Ru loading, 5% Ru/C and 2.6% Ru/TiO_2, have average diameters of 3.3 and 3.9 nm, respectively. By contrast, those with low Ru loading, 0.5% Ru/C and 0.5% Ru/TiO_2, have much smaller diameters of 1.4 and 1.7 nm, respectively. Because the fraction of surface sites with low coordination numbers, such as corners and edges, greatly increases when the particle size is less than 2 nm; although above that the surface is dominated by flat plane terraces,[16] we can consider these four samples as representative of the two extremes: high-coordination flat terraces and low-coordination steps/edges. Chemical bonding of reactants and intermediates on these different types of surface sites during the APR of ethanol is expected to be different, which should result in changes in relative reaction rates and product distribution, as shown below.

Reaction pathways

The product distributions obtained on monometallic and bimetallic Ru and Pt catalysts at ethanol conversions of approximately 10% are shown in Table 2 for the liquid and gas phases. It is observed that acetaldehyde is the main liquid product, although diethyl ether and acetic acid are only significant in some of the catalysts such as 0.5% Ru/TiO_2, 2%

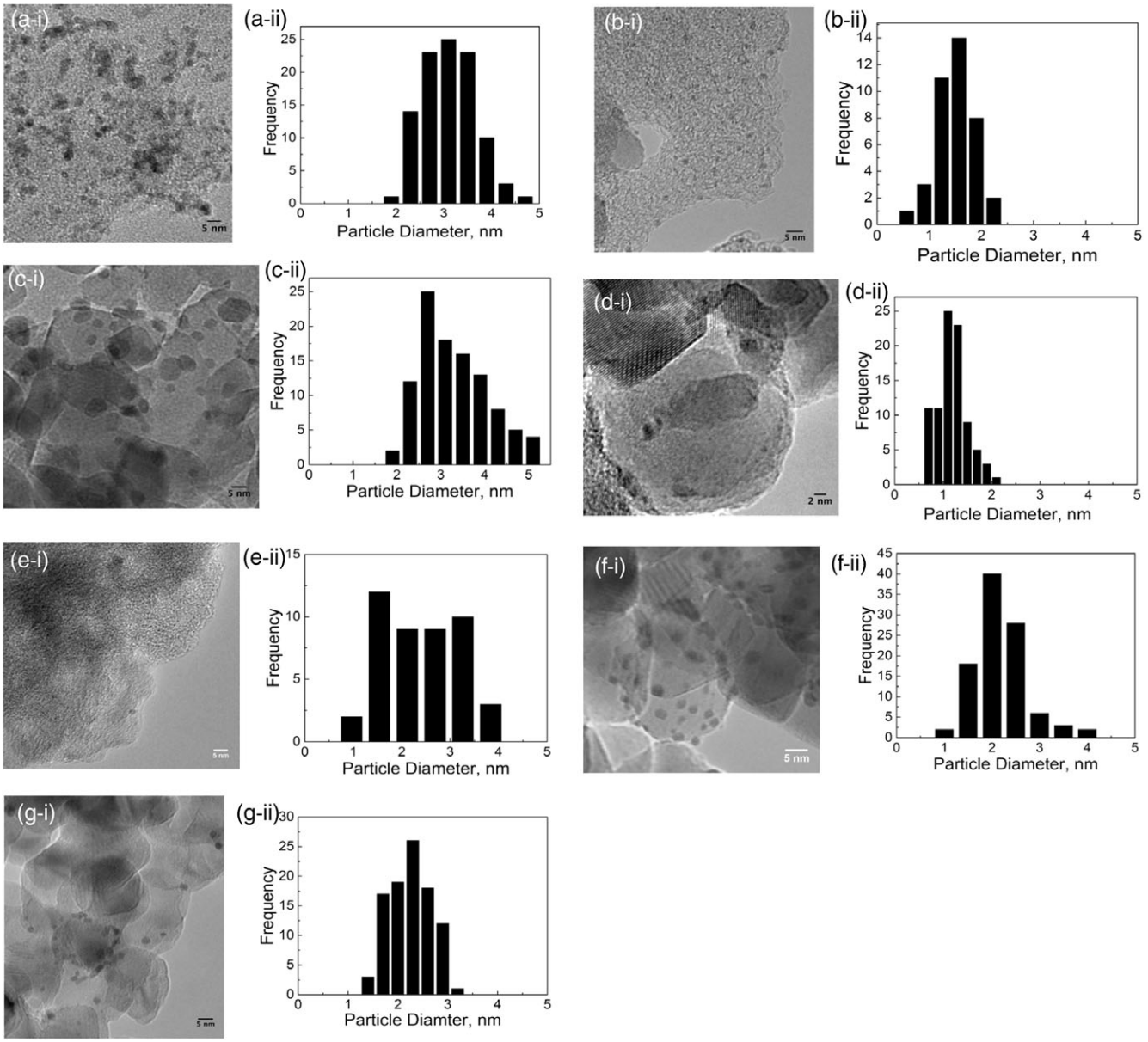

Figure 1. (i) TEM images and (ii) particle diameter distribution of the different catalysts; (a) 5% Ru/C; (b) 0.5% Ru/C; (c) 2.6% Ru/TiO_2; (d) 0.5% Ru/TiO_2; (e) 1% Pt/C; (f) 2% Pt/TiO_2; and (g) 1% Ru–2% Pt/TiO_2.

Table 2. Liquid Phase and Gas Phase Products Distribution of Aqueous Phase Reforming of Ethanol

Sample	Amount (mg)	Time (h)	Conversion (%)	Liquid products (mmol)			Gas products (mmol)					Product ratio	
				Acetaldehyde	Acetic acid	Diethyl ether	H_2	CO_2	CH_4	CO	C_2H_6	C_2H_4	C1/C2	CO_2/CH_4
5% Ru/C	100	1	12	3.82	0.00	0.11	6.93	9.60	33.99	0.72	1.29	0.00	11.59	0.28
0.5% Ru/C	150	3	9	6.75	0.00	1.35	12.13	4.16	8.08	2.00	0.99	0.00	2.11	0.52
2.6% Ru/TiO_2	200	1	11	2.73	0.00	0.02	9.18	9.10	29.56	0.00	3.03	0.00	14.14	0.31
0.5% Ru/TiO_2	200	3	11	8.22	1.06	3.12	18.08	3.58	7.64	0.84	1.38	0.00	1.30	0.47
1% Pt/C	200	1	7	3.36	0.63	0.60	27.30	7.27	10.29	0.00	1.03	0.00	4.40	0.71
2% Pt/TiO_2	200	1	11	3.74	2.54	3.98	28.95	3.26	3.33	0.00	2.06	0.00	1.05	0.98
0.5% Ru/2% Pt/TiO_2	200	1	9	3.55	3.60	1.92	33.04	2.72	2.91	0.00	1.14	0.00	0.79	0.93
2% Pt/0.5% Ru/TiO_2	200	1	13	2.91	4.18	2.80	39.65	8.45	14.74	0.00	1.84	0.00	3.27	0.57
1% Ru–2% Pt/TiO_2	200	0.75	9	1.84	0.00	0.19	44.12	9.10	12.03	0.00	2.75	0.00	11.49	0.76
TiO_2	200	1	1	1.52	0.00	1.49	1.88	0.00	0.00	0.00	0.00	0.29	0	0

Pt/TiO_2, 0.5% Ru/2% Pt/TiO_2, and 2% Pt/0.5% Ru/TiO_2. The gas products contain predominantly H_2, CO_2, and CH_4, with smaller amounts of ethane and ethylene. To analyze the possible reaction pathways on 0.5% Ru/TiO_2, the evolution of liquid products in the batch reactor has been plotted as a function of reaction time (Figure 2). It can be observed that the initial rate of acetaldehyde formation during the first 1 h is 6.6 mmol/h, which is much higher than that of diethyl ether. The formation of acetic acid is not detected by gas chromatography until 3 h on stream. Therefore, it can be concluded that the primary products of ethanol reforming on this catalyst are acetaldehyde and H_2 because of dehydrogenation of ethanol.

Density functional theory (DFT) calculations of oxygenates reforming have been previously conducted over Ru[17,18] and Pt.[19-24] These studies have shown that the adsorption of ethanol is thermodynamically favorable when a surface ethoxy species is formed via dehydrogenation, which starts at the O of ethanol. The elongation of the O—H bond reduces the electron orbital overlap between H and O, leading to the detachment of H from O. This first step is followed by dehydrogenation of the C at the α-position from O and, finally, formation of the adsorbed surface acetaldehyde.[21] The dehydrogenation of the surface acetaldehyde species has been experimentally studied with high-resolution electron energy loss spectroscopy.[25] It has been shown that this step leads to the formation of a surface acetyl species, which are important metastable intermediates. Because there is no more H at the α-position C of surface acetyl species CH_3CO, further dehydrogenation of acetyl species takes place on the C at the β-position.

As a consequence of this sequential dehydrogenation and enhanced interaction with the surface, the C—C bond weakens. It seems like this double dehydrogenation (of O—H and C—H bonds) requires a lower energy barrier than that required for C—C cleavage, which still requires another dehydrogenation step before it can occur. For example, over Ru(0001), the activation energy of C—C cleavage for ethanol decreases from 255 kJ/mol before adsorption to 38 kJ/mol when the surface CH_2CO species is formed.[18] A much lower effect of dehydrogenation occurs with Pt. In fact, the activation energy of C—C cleavage over Pt(111) only decreases to 90.24 kJ/mol after the surface ketenyl CHCO is formed.[22] In comparison, a deeper degree of dehydrogenation is needed over Pt to weaken the C—C bond. Moreover, for both metals, the adsorption geometry of ethanol changes during the dehydrogenation steps.[18,20] The metal—O bond of the surface ethoxy group is tilted upon adsorption, making dehydrogenation of O—H and Cα—H easier than C—C cleavage. However, further dehydrogenation of Cβ leads to a parallel adsorption geometry that weakens the metal—O bond. As O moves away from the surface, C—O cleavage becomes much harder.

Cleavage of the C—C bond results in the formation of CH_4 and CO with a molar ratio of 1. As shown in Table 2, CH_4 is observed as a product for all catalysts, but its relative abundance varies among different catalysts. By contrast, CO is not a significant product for any of the catalysts investigated. CO has been observed as a major product in several studies.[26,27] However, under the current reaction conditions (523.15 K and a high water/ethanol molar ratio (18:1), the WGS reaction is thermodynamically favored,[28] and consequently CO rapidly reacts with water, yielding CO_2 and H_2.

Because the C—C cleavage of ethanol should produce an equimolar ratio of CO to CH_4, any deviation from an equimolar CO_2/CH_4 ratio should be ascribed to methanation of H_2 and CO_2 to CH_4. The observed CO_2/CH_4 ratio is much less than one for nearly all catalysts. On 5% Ru/C, this ratio is

9.6 mmol/33.99 mmol (0.28). If CH_4 were only produced by C—C cleavage of ethanol, the amount of H_2 produced from the WGS reaction should be 33.99 mmol. However, the total H_2 is only 6.93 mmol, clearly showing that H_2 and CO_2 undergo conversion to CH_4. It is known that Pt and Ru have different activities toward methanation.[29,30] Ru is much more active for methanation. Thus, the observed CO_2/CH_4 ratio can be taken as a figure of merit when assessing different catalysts for the APR of ethanol.

As depicted in Scheme 1, the low temperature APR of ethanol over Ru and Pt involves the following steps. First, ethanol is dehydrogenated to form a surface aldehyde species, which either desorbs into the liquid phase or undergoes hydration and further dehydrogenation to produce acetic acid. Although this path generates H_2, it does not include C—C cleavage and consequently does not produce the maximum yield of H_2. By contrast, if the surface aldehyde species undergoes C—C cleavage via decarbonylation, CH_4 and CO are produced at a 1:1 ratio. In a subsequent step, adsorbed CO alternatively undergoes the water–gas shift reaction producing CO_2 and H_2 or methanation. A parallel path that does not produce H_2 is the dehydration–etherification that leads to diethyl ether. Another possible product is ethane, which is obtained by dehydration of ethanol to ethylene followed by hydrogenation.

Ru particle size effects

To evaluate the effect of particle size on Ru catalysts, liquid- and gas-phase product distributions are compared at early stages of reaction (approximately 10% conversion) for the different monometallic Ru catalysts, as listed in Table 2. The greatest differences in the Ru series are observed in the gas-phase product distributions (see Figure 3). The catalysts with higher Ru loading and larger particle sizes produce more CH_4 than H_2. The CH_4/H_2 molar ratios for 5% Ru/C and 2.6% Ru/TiO_2 are 5 and 3, respectively. By contrast, on the lower loading, smaller particle size catalysts, 0.5% Ru/C and 0.5% Ru/TiO_2, the CH_4/H_2 ratio is less than 1, indicating that the reaction selectively produces H_2 rather than CH_4. These results are consistent with previous studies conducted at 473.15 K,[31] in which the CH_4/H_2 ratio was 3.3 over a 5% Ru/TiO_2 catalyst and 0.4 over 0.5% Ru/TiO_2.

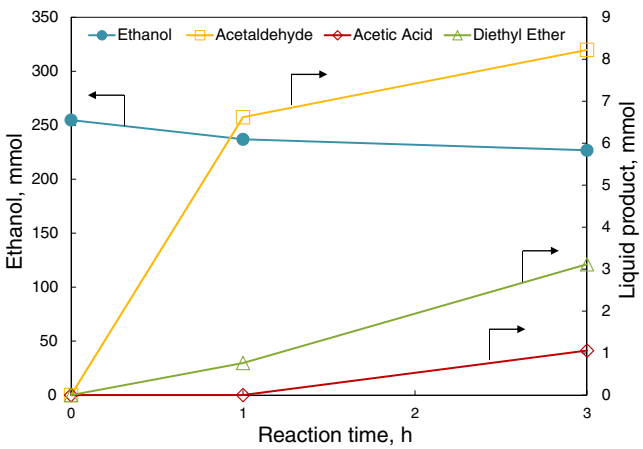

Figure 2. Liquid product distribution of 0.5% Ru/TiO_2 catalysts as a function of reaction time. Reaction conditions: 200 mg of catalyst, 523.15 K, 1.38 Mpa of Ar; feed: 15 vol % ethanol aqueous solution with overall volume of 100 mL.

[Color figure can be viewed at wileyonlinelibrary.com]

Another important figure of merit to evaluate catalyst performance is the C1/C2 product ratio, listed in Table 2, which is a measure of the relative ability of the catalyst to achieve C—C bond cleavage. Higher C1/C2 ratio indicates more C1 products, for example, CO, CO_2, and CH_4, in the gas phase. Similarly, liquid products such as acetaldehyde and acetic acid make up for C2 products, and a low C1/C2 ratio signifies that ethanol has further reacted, mainly to liquid products. Our experimental results clearly show that the C1/C2 product ratio is higher on the catalysts with larger particle sizes (i.e., 5% Ru/C and 2.6% Ru/TiO_2). However, DFT calculation shows that the energy barriers for C—C bond cleavage are lower on low-coordination-number sites at the corners and step-edges on metal surfaces.[32-34] A possible explanation could be that the more active, low-coordination sites are more likely to be blocked by the fragment produced during the initial C—C cleavage and the binding of these fragments (CO or CH_x) is too strong to easily react with H_2 and regenerate the active site.[17] Other possible deactivation mechanisms are attributed to reactions such as the Boudouard reaction, methane decomposition, ethylene polymerization, and cracking of ethane.[5,35] Among them, the carbon deposition via the Boudouard reaction ($2CO = CO_2 + C$) is the most commonly proposed. However, the solid carbon formation under excess water and low temperatures is thermodynamically unfavorable.[36,37]

The phenomenon of site blocking by CO was further demonstrated by investigating the FTS reaction in the aqueous phase over the two catalysts, 5% Ru/C and 0.5% Ru/C. This is a good probe reaction, because it involves C—O dissociation as the rate-limiting step. For comparison, the same conditions used in the APR of ethanol were used for the FTS, with the only difference being in the composition of the gas phase, for the reaction with a H_2/CO molar ratio of 5. Interestingly, the 0.5% Ru/C catalyst produced mainly CO_2 and additional H_2, via WGS reaction. By contrast, CO_2 was not observed as a product over 5% Ru/C. Instead, C_1–C_7 alkanes were the main products observed. These results clearly indicate that the smaller particles present on 0.5% Ru/C are deactivated by CO to a greater extent. That is, the low-coordination corner and step sites present in smaller Ru particles adsorb CO more strongly and are quickly rendered inactive. CO activation is hard to achieve. The FTS is hindered over low coordinate step edge sites. However, for 5% Ru/C, surface CO is more easily activated over with larger Ru particles. By contrast, adsorption of CO and CO_2 on the high-coordinate surface sites is much weaker; therefore, these sites are kept clean and active for C—O dissociation and subsequent C—C bond formation to longer chain hydrocarbons.

Carballo et al.[38] investigated Ru particle size effects on the FTS ranging from 4 to 23 nm. The turnover frequencies (TOF) for H_2 and CO as well as CH_4 formation increased with particle sizes smaller than 10 nm. The DFT calculation by Loveless et al.[39,40] suggests that the energy barriers of chemisorbed CO activation on the low-coordinated corner and step-edge sites are larger than on the high-coordinated flat-extended surface. H-assisted CO activation on Ru(111) terrace of Ru_{201} cluster lowers the activation energy to 165 kJ/mol compared to 356 kJ/mol for CO activation without H-assistance at corner sites. Strong adsorption of CO at the corner and step-edge sites significantly blocks the Ru active sites.

Pt particle size effects

All monometallic Pt catalysts exhibit high selectivity toward H_2 and low selectivity to CH_4. The results are plotted in

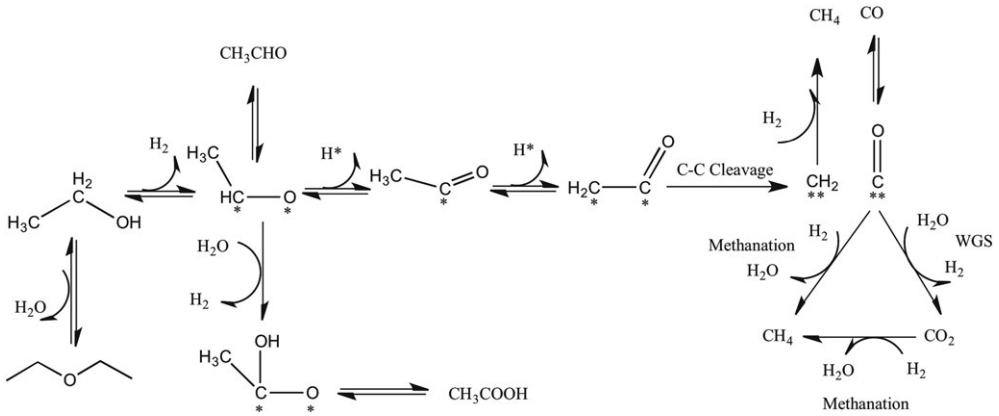

Scheme 1. Reaction pathways of the low temperature aqueous phase reforming of ethanol.

Figure 4. Liquid products such as acetaldehyde, acetic acid, and diethyl ether are noteworthy. However, as demonstrated by DFT calculations, ethanol decomposition via C—C cleavage is more difficult on Pt[22] than on Ru,[18] as revealed by the calculated energy barriers, 90 kJ/mol for Pt, compared to 38 kJ/mol for Ru. Moreover, the C—C cleavage over Pt happens after the surface ketenyl CHCO species via dehydrogenation of Cβ is formed indicating the stronger affinity of Pt for H atoms. Therefore, one should expect that most of the H_2 produced over Pt catalysts derives from dehydrogenation of ethanol. However, because no CO is observed in the gas phase products when Pt is present because of the favorable WGS reaction at low temperatures, one can expect that surface CO converts to CO_2 producing additional H_2. This observation is consistent with previous results of WGS reactions,[41] showing that the TOF over Pt is about six times higher than over Ru for the same reaction temperatures.

For Pt catalysts, increasing the metal loading from 1 to 2 wt % did not result in a significant change in particle size, as shown in the TEM images and particle size distributions of Figure 1e,f, that is, 2.2 nm for 1% Pt/C and 2.4 nm for 2% Pt/TiO_2. The product distributions on these two catalysts were similar, with the 1% Pt/C catalysts producing only slightly more CO_2 and CH_4. Contrasting with Ru, Pt exhibits a lower activity toward the methanation reaction.[29] Indeed, DFT calculations suggest a high activation energy barrier for CO dissociation on a Pt(111) surface with a C—O bond length close to the value for free CO.[42] Therefore, CH_4 production is practically negligible on Pt. However, the adsorption and decomposition of ethanol, acetaldehyde, and glycerol have been previously investigated over Pt catalysts of different particle size and different planes of Pt single crystals. For instance, Cong et al.[43] has investigated the adsorption and desorption of ethanol on Pt(331), which consists of steps and terraces of Pt(111). The step sites display high activity for direct C—C cleavage upon adsorption, although terrace sites catalyze the dehydrogenation of ethanol, followed by C—C cleavage. Likewise, the decomposition of acetaldehyde has been studied over Pt catalysts of different particle sizes,[44] with the observation that large particles exhibit a lower activity toward C—C cleavage, reflected by a lower rate of acetaldehyde decomposition. Pt particle size effects have also been studied in the APR of glycerol[44,45] with the smaller Pt particles producing a higher selectivity to CH_4 and C1 oxygenates. Several experimental studies concluded that WGS reactivity on Pt is independent of particle size.[41,46]

Effect of the support

Supports are not only used to disperse metal particles, but they may also promote catalytic activity for some reactions.

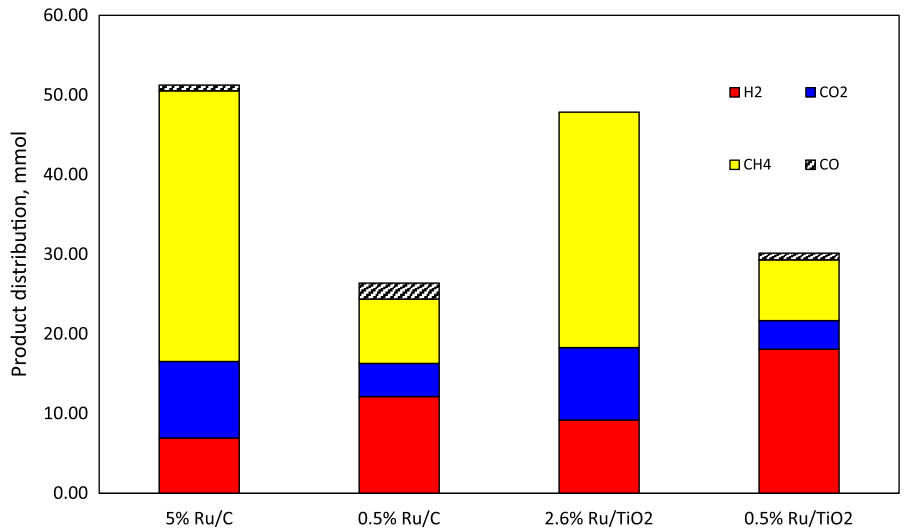

Figure 3. Gas phase product distribution over different Ru catalysts. Reaction conditions: 523.15 K, 1.38 Mpa of Ar; feed: 15 vol % ethanol aqueous solution with overall volume of 100 mL.

[Color figure can be viewed at wileyonlinelibrary.com]

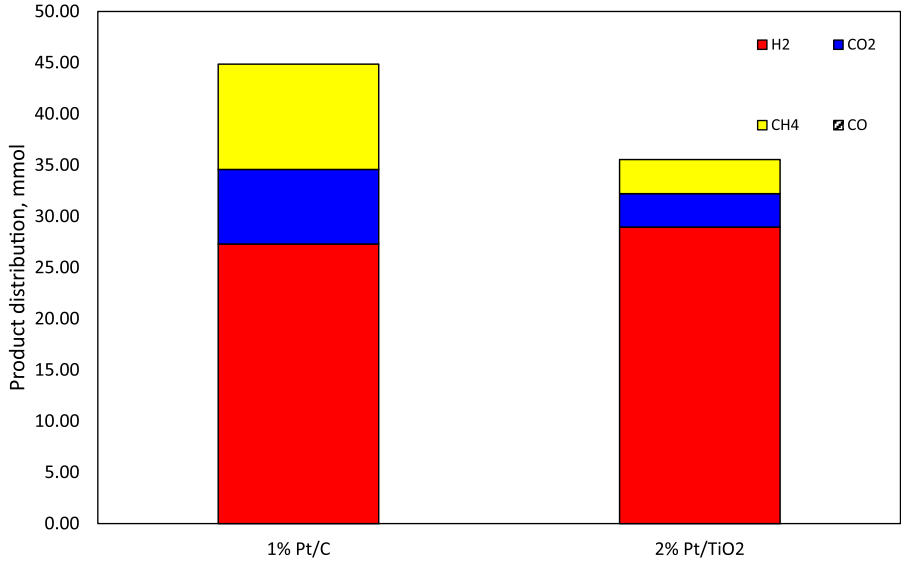

Figure 4. Gas phase product distribution over different Pt catalysts. Reaction conditions: 523.15 K, 1.38 Mpa of Ar; feed: 15 vol % ethanol aqueous solution with overall volume of 100 mL.
[Color figure can be viewed at wileyonlinelibrary.com]

Our experimental results, summarized in Table 2, indicate that the bare TiO_2 support catalyzes dehydrogenation and dehydration reactions under ethanol APR reaction conditions. Dehydrogenation of ethanol produces H_2 and acetaldehyde, whereas dehydration of ethanol yields diethyl ether and ethylene, which are observed in moderate amounts. By contrast, no CO, CO_2, or CH_4 is detected, indicating that TiO_2 has no activity for C—C bond cleavage.

TiO_2 exhibits a higher activity toward ethanol conversion than the carbon support, most probably via acid–base interactions. It is possible that an H atom of ethanol, acting as an acid, may interact with a basic site of TiO_2, whereas the O atom of ethanol may interact with a surface Ti^{4+} site having Lewis acidity.[47] As a result, an ethoxide is formed on the surface of TiO_2. Under the presence of water, the surface ethoxide may further interact with surface OH groups, further dehydrogenating to acetaldehyde,[35,47,48] which can in turn reacts to form a surface acetate. When a metal is supported on TiO_2, bifunctional activity may develop.[35,45] It has been proposed that the acetate species can decompose at the metal–support interface, producing CO, which can undergo WGS reaction, yielding CO_2 and H_2. Guo et al.[49] has suggested that strong basic sites present on a support could promote the dissociation of water, facilitating the WGS. This idea is consistent with our experimental results (see Table 2), which show that carbon-supported Ru produces much more CO in the gas phase than TiO_2-supported Ru. That is, the sequential conversion of CO to CO_2 via the WGS reaction is not promoted on the carbon support as it is on TiO_2.

Bimetallic Ru–Pt catalysts

Based on the results shown above, we have selected the bimetallic Ru–Pt catalysts supported on TiO_2 as potentially promising materials that may incorporate the beneficial properties of the support as well as both Ru and Pt, without the negative effects of either. That is, the TiO_2 support may enhance C2 decomposition as well as WGS, whereas Ru catalyzes C—C cleavage, and Pt enhances WGS. However, we have shown that flat Ru surfaces with large Ru ensembles may promote the undesired methanation reaction that consumes H_2 and produces CH_4, which is detrimental. At the same time, small Ru particles may lead to strong adsorption of CO at the low-coordination corner and step-edge sites, poisoning the sites. Alloying Ru with Pt, however, may simultaneously result in lower density of large Ru ensembles and lower density of uncoordinated defects. Pt itself has low activity toward C—C cleavage but enhanced activity for the WGS.

Table 2 summarizes the results of the APR over the three bimetallic catalysts. Two of them are the sequentially impregnated bimetallics (one Ru first, the other Pt first), whereas the third one is the co-impregnated (Ru–Pt). The product distributions observed in the gas phase are presented in Figure 5. The behavior of the bimetallic 0.5% Ru/2% Pt/TiO_2 (Ru first) resembles that of the monometallic 2% Pt/TiO_2. This result would suggest that the small Ru loading (0.5%) deposited first on the support becomes covered by the larger amount of Pt (2%), without much Ru exposure. In the reversed preparation sequence, 2% Pt/0.5% Ru/TiO_2 (Pt first), the added Ru provides enhanced C—C bond cleavage, producing surface CO. The abundant liquid products indicate that there are still large fractions of exposed Pt that catalyze dehydrogenation and not enough exposed Ru to break C—C bonds. However, the co-impregnated 2% Pt–1% Ru/TiO_2, with higher Ru loading, demonstrates an excellent performance providing sufficient C—C cleavage activity upon ethanol adsorption and high WGS activity to convert the surface CO species to CO_2 and H_2 without undergoing methanation. Aiming to detect any interaction between Pt and Ru in the bimetallic Pt–Ru/TiO_2 catalyst, the XRD patterns of 2% Pt/TiO_2, 1% Ru/TiO_2, and 2% Pt–1% Ru/TiO_2 were recorded (see Figure 6). However, only TiO_2 diffraction peaks representing the anatase and rutile forms were detected for those three catalysts. Pt and Ru intensities were too weak to be used as a measure of Pt–Ru interactions. This is because the low loading of Pt and Ru as well as their high dispersion on TiO_2. A weak peak was observed at 2θ of 40.0° for 2% Pt–1% Ru/TiO_2 (line a) and 2% Pt/TiO_2 (line b) catalysts. As depicted in line d, after subtracting the 1% Ru/TiO_2 (line c) from 2% Pt–1% Ru/TiO_2 (line a), a weak intensity emerged. This peak corresponds to the Pt(111) diffraction. Similarly, subtracting 1% Ru/TiO_2 (line c) from 2%

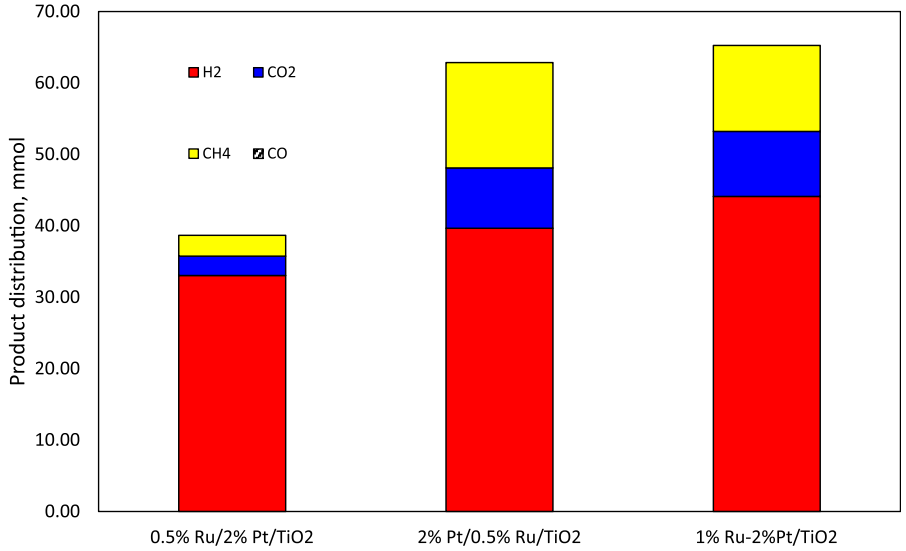

Figure 5. Gas phase product distribution over different Pt–Ru bimetallic catalysts. Reaction conditions: 523.15 K, 1.38 Mpa of Ar; feed: 15 vol % ethanol aqueous solution with overall volume of 100 mL.

[Color figure can be viewed at wileyonlinelibrary.com]

Pt/TiO_2 (line b) should have resulted diffraction patterns for monometallic Pt in line e. However, the intensities for both lines d and e are too similar to identify any Pt–Ru interaction. The same analysis is also conducted to identify Ru diffraction patterns. As indicated in line f, no noticeable intensities have been detected.

Bimetallic Pt–Ru catalysts have been found to be effective for APR of biomass, with high catalytic activity toward H_2 production.[50,51] The multi-objective optimization diagram presented in Figure 7 provides a comprehensive perspective with full assessment of optimal catalysts toward this reaction.

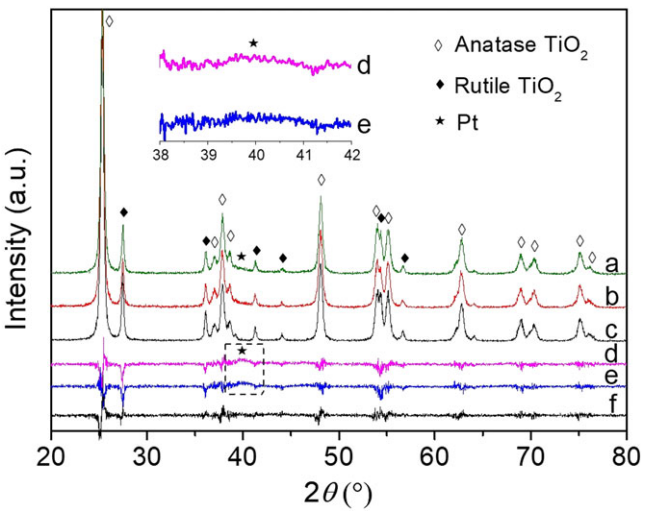

Figure 6. XRD patterns for prereduced 2% Pt–1% Ru/TiO_2 as line "a;" 2% Pt/TiO_2 as line "b;" 1% Ru/TiO_2 as line "c." The line "d" shows the difference in intensity between 2% Pt–1% Ru/TiO_2 and 1% Ru/TiO_2; the line "e" shows the difference in intensity between 2% Pt/TiO_2 and 1% Ru/TiO_2, whereas the line "f" shows the difference in intensity between 2% Pt–1% Ru/TiO_2 and 2% Pt/TiO_2.

[Color figure can be viewed at wileyonlinelibrary.com]

Catalysts can be compared on the basis of their H_2 production rate (per gram of catalyst) along with the ratio of CO_x to C2 products. CO_x represents the sum of CO_2 and CO; C2 represents the total amount of two-carbon products. The ratio of CO_x-to-C2 provides a measure of the efficiency of each catalyst for C—C cleavage. Catalyst with maximum potential for APR of ethanol should maximize the yield of H_2 per unit time with maximum utilization of the carbon source. It is clear that all the points for the pure Ru series are located to the left side of the diagram, which is less desirable. Although Ru is efficient at C—C cleavage readily converting C2 products into C1 products, the yield of H_2 production is rather low. Large Ru particles tend to dissociate CO easily and produce CH_4 by consuming H_2. At the same time, smaller Ru particles strongly adsorb of CO which is difficult to further react and leads to site poisoning. However, while Pt catalysts produce significant

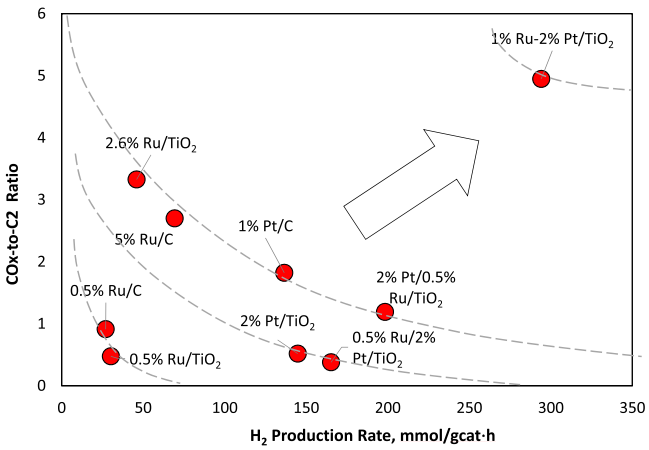

Figure 7. Assessment of catalyst performances based on two desirable ratios: vertical: CO_x-to-C2 ratio, which indicates the catalyst efficiency for C—C cleavage; horizontal: overall H_2 production rate. The optimal catalysts should appear on the upper right corner of the diagram.

[Color figure can be viewed at wileyonlinelibrary.com]

amounts of H_2, this conversion is mainly through dehydrogenation of ethanol. Therefore, although the H_2 production rate is higher than on Ru catalysts, the utilization of ethanol is incomplete. That is, the low CO_x-to-C2 ratios observed for pure Pt catalysts indicates that large amounts of C2 liquid products are required to obtain a given H_2 yield. Finally, the bimetallic catalysts display their points toward to upper right of the diagram because the efficiency of the C—C cleavage is enhanced, and the produced CO is further converted via WGS reaction, mostly catalyzed by Pt, which results in maximum H_2 production rate with maximum utilization of ethanol.

Conclusions

Monometallic Ru catalysts with large particle sizes display high activity toward C—C cleavage upon ethanol adsorption. However, the larger Ru particles more readily dissociate CO which reacts with H_2 to form CH_4. Smaller Ru particle shows higher selectivity toward H_2, but the CO species present strong adsorption on low index corner step-edge sites lowers the overall catalytic activity because of site poisoning. On the contrary, Pt also reveals high selectivity toward H_2 production and lower activity to methanation reaction. The surface CO species react with water via WGS reaction to produce more H_2 and CO_2. However, the activation energy of C—C cleavage over Pt is much higher than that over Ru, making ethanol reforming less efficient.

Support TiO_2 interacts strongly with ethanol and water through acid–base interaction. Ethanol decomposes upon adsorption and produced acetaldehyde as the dehydrogenation product and ethylene along with diethyl ether as dehydration products. The basicity of TiO_2 is also believed to promote the WGS reaction.

Bimetallic Ru–Pt with 1% Ru co-impregnated with 2% Pt over TiO_2, located at the top right of the optimization diagram, exhibited the beneficial properties of both Ru and Pt without the negative effects of either. Its synergistic behavior results in higher H_2 production rate, higher C—C cleavage ability, and lower methanation rate than any of the monometallic Ru or Pt catalysts.

Acknowledgments

This research has been funded by Abengoa Research.

Literature Cited

1. Barreto L, Makihira A, Riahi K. The hydrogen economy in the 21st century: a sustainable development scenario. *Int J Hydrogen Energy*. 2003;28(3):267-284.
2. Cortright R, Davda R, Dumesic JA. Hydrogen from catalytic reforming of biomass-derived hydrocarbons in liquid water. *Nature*. 2002; 418(6901):964-967.
3. Davda R, Shabaker J, Huber G, Cortright R, Dumesic JA. A review of catalytic issues and process conditions for renewable hydrogen and alkanes by aqueous-phase reforming of oxygenated hydrocarbons over supported metal catalysts. *Appl Catal Environ*. 2005;56(1):171-186.
4. Haryanto A, Fernando S, Murali N, Adhikari S. Current status of hydrogen production techniques by steam reforming of ethanol: a review. *Energy Fuel*. 2005;19(5):2098-2106.
5. Ni M, Leung DY, Leung MK. A review on reforming bio-ethanol for hydrogen production. *Int J Hydrogen Energy*. 2007;32(15):3238-3247.
6. Liguras DK, Kondarides DI, Verykios XE. Production of hydrogen for fuel cells by steam reforming of ethanol over supported noble metal catalysts. *Appl Catal Environ*. 2003;43(4):345-354.
7. Zhang B, Tang X, Li Y, Xu Y, Shen W. Hydrogen production from steam reforming of ethanol and glycerol over ceria-supported metal catalysts. *Int J Hydrogen Energy*. 2007;32(13):2367-2373.
8. Huber GW, Dumesic JA. An overview of aqueous-phase catalytic processes for production of hydrogen and alkanes in a biorefinery. *Catal Today*. 2006;111(1):119-132.
9. Rabe S, Nachtegaal M, Ulrich T, Vogel F. Towards understanding the catalytic reforming of biomass in supercritical water. *Angew Chem Int Ed*. 2010;49(36):6434-6437.
10. Petrović Ž, Ristić M, Marciuš M, et al. Formation of RuO_2 nanoparticles by thermal decomposition of $Ru(NO)(NO_3)_3$. *Ceram Int*. 2015; 41(6):7811-7815.
11. Nie L, Resasco DE. Kinetics and mechanism of m-cresol hydrodeoxygenation on a Pt/SiO_2 catalyst. *J Catal*. 2014;317:22-29.
12. Omotoso T, Boonyasuwat S, Crossley SP. Understanding the role of TiO_2 crystal structure on the enhanced activity and stability of Ru/TiO_2 catalysts for the conversion of lignin-derived oxygenates. *Green Chem*. 2014;16(2):645-652.
13. Vannice MA, Joyce WH. *Kinetics of Catalytic Reactions*. Vol 134. Springer; 2005.
14. Tokarev A, Kirilin A, Murzina E, et al. The role of bio-ethanol in aqueous phase reforming to sustainable hydrogen. *Int J Hydrogen Energy*. 2010;35(22):12642-12649.
15. Wetchakun N, Incessungvorn B, Wetchakun K, Phanichphant S. Influence of calcination temperature on anatase to rutile phase transformation in TiO_2 nanoparticles synthesized by the modified sol–gel method. *Mater Lett*. 2012;82:195-198.
16. Van Santen RA. Complementary structure sensitive and insensitive catalytic relationships. *Acc Chem Res*. 2008;42(1):57-66.
17. Ferrin P, Simonetti D, Kandoi S, et al. Modeling ethanol decomposition on transition metals: a combined application of scaling and Brønsted–Evans–Polanyi relations. *J Am Chem Soc*. 2009;131(16): 5809-5815.
18. C-c C, Genest A, Rösch N. Decomposition of ethanol over Ru (0001): a DFT study. *Top Catal*. 2013;56(11):874-884.
19. Alcala R, Mavrikakis M. Dumesic JA. DFT studies for cleavage of C-C and C-O bonds in surface species derived from ethanol on Pt (111). *J Catal*. 2003;218(1):178-190.
20. Dancini-Pontes I, Fernandes-Machado NR, de Souza M, Pontes RM. Insights into ethanol decomposition over Pt: a DFT energy decomposition analysis for the reaction mechanism leading to C_2H_6 and CH_4. *Appl Catal Gen*. 2015;491:86-93.
21. Gursahani KI, Alcalá R, Cortright RD, Dumesic JA. Reaction kinetics measurements and analysis of reaction pathways for conversions of acetic acid, ethanol, and ethyl acetate over silica-supported Pt. *Appl Catal Gen*. 2001;222(1):369-392.
22. Sutton JE, Panagiotopoulou P, Verykios XE, Vlachos DG. Combined DFT, microkinetic, and experimental study of ethanol steam reforming on Pt. *J Phys Chem C*. 2013;117(9):4691-4706.
23. Liu B, Greeley J. Density functional theory study of selectivity considerations for C–C versus C–O bond scission in glycerol decomposition on Pt (111). *Top Catal*. 2012;55(5–6):280-289.
24. Coslovich G, Vesselli E. Modelling of ethanol decomposition on Pt (111): a comparison with experiment and density functional theory. *J Phys Condens Matter*. 2005;(39):6139-6148.
25. Henderson MA, Zhou Y, White J. Polymerization and decomposition of acetaldehyde on rutherium (001). *J Am Chem Soc*. 1989;111(4): 1185-1193.
26. Ciambelli P, Palma V, Ruggiero A. Low temperature catalytic steam reforming of ethanol. 2. Preliminary kinetic investigation of Pt/CeO_2 catalysts. *Appl Catal Environ*. 2010;96(1):190-197.
27. Rossi C, Alonso C, Antunes O, Guirardello R, Cardozo-Filho L. Thermodynamic analysis of steam reforming of ethanol and glycerine for hydrogen production. *Int J Hydrogen Energy*. 2009;34(1):323-332.
28. Smith R, Loganathan M, Shantha MS. A review of the water gas shift reaction kinetics. *Int J Chem React Eng*. 2010;8(1).
29. Vannice M. The catalytic synthesis of hydrocarbons from H2CO mixtures over the group VIII metals: V. The catalytic behavior of silica-supported metals. *J Catal*. 1977;50(2):228-236.
30. Wei W, Jinlong G. Methanation of carbon dioxide: an overview. *Front Chem Sci Eng*. 2011;5(1):2-10.
31. Nozawa T, Mizukoshi Y, Yoshida A, Naito S. Aqueous phase reforming of ethanol and acetic acid over TiO_2 supported Ru catalysts. *Appl Catal Environ*. 2014;146:221-226.
32. Chen Y, Vlachos DG. Hydrogenation of ethylene and dehydrogenation and hydrogenolysis of ethane on Pt (111) and Pt (211): a density functional theory study. *J Phys Chem C*. 2010;114(11):4973-4982.

33. Watwe RM, Cortright RD, Nørskov JK, Dumesic JA. Theoretical studies of stability and reactivity of C2 hydrocarbon species on Pt clusters, Pt (111), and Pt (211). *J Phys Chem B*. 2000;104(10):2299-2310.
34. Yang M-L, Zhu Y-A, Fan C, Sui Z-J, Chen D, Zhou X-G. DFT study of propane dehydrogenation on Pt catalyst: effects of step sites. *Phys Chem Chem Phys*. 2011;13(8):3257-3267.
35. Hou T, Zhang S, Chen Y, Wang D, Cai W. Hydrogen production from ethanol reforming: catalysts and reaction mechanism. *Renew Sustain Energy Rev*. 2015;44:132-148.
36. Garcia E, Laborde M. Hydrogen production by the steam reforming of ethanol: thermodynamic analysis. *Int J Hydrogen Energy*. 1991;16(5):307-312.
37. Liu S, Zhang K, Fang L, Li Y. Thermodynamic analysis of hydrogen production from oxidative steam reforming of ethanol. *Energy Fuel*. 2008;22(2):1365-1370.
38. Carballo JMG, Yang J, Holmen A, et al. Catalytic effects of ruthenium particle size on the Fischer–Tropsch synthesis. *J Catal*. 2011;284(1):102-108.
39. Loveless B. *CO Bond Activation and CC Bond Formation Paths in Catalytic CO Hydrogenation [doctoral dissertation]*. Berkeley: University of California; 2012.
40. Loveless BT, Buda C, Neurock M, Iglesia E. CO chemisorption and dissociation at high coverages during CO hydrogenation on Ru catalysts. *J Am Chem Soc*. 2013;135(16):6107-6121.
41. Panagiotopoulou P, Kondarides DI. Effect of morphological characteristics of TiO_2-supported noble metal catalysts on their activity for the water–gas shift reaction. *J Catal*. 2004;225(2):327-336.
42. Souza Monteiro R, Paes LW, M Carneiro JW, Aranda DA. Modeling the adsorption of CO on small Pt, Fe and Co clusters for the Fischer-Tropsch synthesis. *J Cluster Sci*. 2008;19(4):601-614.
43. Cong Y, Van Spaendonk V, Masel R. Low temperature C-C bond scission during ethanol decomposition on Pt (331). *Surf Sci*. 1997; 385(2):246-258.
44. Ciftci A, Michel D, Hensen EJ. Influence of Pt particle size and Re addition by catalytic reduction on aqueous phase reforming of glycerol for carbon-supported Pt (Re) catalysts. *Appl Catal Environ*. 2015;174: 126-135.
45. Wawrzetz A, Peng B, Hrabar A, Jentys A, Lemonidou A, Lercher J. Towards understanding the bifunctional hydrodeoxygenation and aqueous phase reforming of glycerol. *J Catal*. 2010; 269(2):411-420.
46. Kalamaras CM, Americanou S, Efstathiou AM. "Redox" vs "associative formate with–OH group regeneration" WGS reaction mechanism on Pt/CeO_2: effect of platinum particle size. *J Catal*. 2011;279(2): 287-300.
47. Rasko J, Hancz A, Erd□helyi A. Surface species and gas phase products in steam reforming of ethanol on TiO 2 and Rh/TiO 2. *Appl Catal Gen*. 2004;269(1):13-25.
48. Jacobs G, Keogh RA, Davis BH. Steam reforming of ethanol over Pt/ceria with co-fed hydrogen. *J Catal*. 2007;245(2):326-337.
49. Guo Y, Azmat MU, Liu X, Wang Y, Lu G. Effect of support's basic properties on hydrogen production in aqueous-phase reforming of glycerol and correlation between WGS and APR. *Appl Energy*. 2012; 92:218-223.
50. Chang AC-C, Louh R, Wong D, Tseng J, Lee Y. Hydrogen production by aqueous-phase biomass reforming over carbon textile supported Pt–Ru bimetallic catalysts. *Int J Hydrogen Energy*. 2011;36(14):8794-8799.
51. D'Angelo MN, Ordomsky V, van der Schaaf J, Schouten J, Nijhuis T. Continuous hydrogen stripping during aqueous phase reforming of sorbitol in a washcoated microchannel reactor with a Pt–Ru bimetallic catalyst. *Int J Hydrogen Energy*. 2014;39(31):18069-18076.

Manuscript received Jan. 19, 2018, and revision received Sep. 10, 2018.